Crystal structure, local structure, and defect structure of Pr-doped SrTiO$_3$

I. A. Sluchinskaya,[1,a)] A. I. Lebedev,[1] and A. Erko[2]
[1]*Moscow State University, Physics Department, Leninskie Gory, 119991 Moscow, Russia*
[2]*Helmholtz-Zentrum Berlin, Albert-Einstein-Str. 15, 12489 Berlin, Germany*

X-ray diffraction studies showed that the structure of $(Sr_{1-x}Pr_x)TiO_3$ solid solutions at 300 K changes from the cubic $Pm3m$ to the tetragonal $I4/mcm$ with increasing x. The analysis of XANES and EXAFS spectra of the solid solutions revealed that Pr ions are predominantly in the 3+ oxidation state, they substitute for Sr atoms and are on-center regardless of the preparation conditions. The weak dependence of the lattice parameter in $(Sr_{1-x}Pr_x)TiO_3$ on the Pr concentration was explained by the competition between the relaxation of the Sr–O bond length, which results from the difference in ionic radii of Sr and Pr ions, and the repulsion of positively charged Pr^{3+} and Ti^{4+} ions. It was shown that the most important defects in the crystals are charged Sr vacancies and SrO planar faults; praseodymium does not enter the Sr sites in the planar faults. © 2012 American Institute of Physics. [http://dx.doi.org/10.1063/1.4737586]

I. INTRODUCTION

Strontium titanate SrTiO$_3$ is a perovskite-type crystal widely used in electronics and optoelectronics. Because of its high room-temperature dielectric constant ($\sim$300) that strongly depends on the electric field, strontium titanate is used as a high-k gate dielectric in field-effect transistors and electric-field-tunable capacitors working at microwaves.

Interesting luminescence properties of rare-earth-doped strontium titanate have long been a subject of intensive studies. In particular, doping SrTiO$_3$ with Pr is known to result in the red luminescence. Although the luminescence of SrTiO$_3$(Pr) itself is rather weak, co-doping the samples with oxides of the group-III elements (Al, B, Ga, In) enhances the luminescence efficiency up to 200 times.[1,2] Red-emitting SrTiO$_3$(Pr^{3+}, Al) phosphors are now promising materials for field-emission and vacuum fluorescent displays. However, the influence of co-doping on luminescent properties and the nature of defects acting as non-radiative centers in Pr-doped SrTiO$_3$ are not well understood. The mechanisms responsible for maintaining charge neutrality in this material have not been identified yet.

Strontium titanate is a model system for studying physical phenomena resulting in ferroelectricity. It is an incipient ferroelectric with a cubic $Pm3m$ structure at 300 K, in which quantum fluctuations stabilize the paraelectric phase up to the lowest temperatures. At about 105 K SrTiO$_3$ undergoes the structural (antiferrodistortive) $Pm3m \rightarrow I4/mcm$ phase transition associated with the oxygen octahedra rotations.[3] This transition is, however, of nonpolar character and weakly influences the dielectric properties. Ferroelectricity in SrTiO$_3$ can be induced by the application of external electric[4] or strain fields,[5] doping with impurities,[6–8] or isotope substitution.[9] Due to the large lattice polarizability, SrTiO$_3$ is very sensitive to doping. The substitution of Sr^{2+} with Pb^{2+}, Ba^{2+}, Ca^{2+}, Cd^{2+}, Mn^{2+}, and Bi^{3+} ions strongly influences the dielectric properties of SrTiO$_3$ and can induce various types of polar phases (dipole glass, ferroelectric).[10–14] In most cases, however, the temperature of the ferroelectric phase transition in doped SrTiO$_3$ is lower than 300 K.

It was recently reported that the ferroelectric phase transition temperature in Pr-doped SrTiO$_3$ can exceed 300 K.[15] In $(Sr_{1-x}Pr_x)TiO_3$ samples with $x = 0.025$–0.075 Duran *et al.* observed a dielectric anomaly at about 515 K and dielectric hysteresis loops at room temperature, which were attributed to the ferroelectric phase transition. The crystal structure of the samples, however, remained cubic at 300 K, and the temperature of the dielectric anomaly changed by only 10 K when the Pr concentration was increased by three times. This influence of Pr doping differs significantly from the influence of other impurities on the temperature of the ferroelectric phase transition in doped SrTiO$_3$.[10–13] According to the XPS spectra,[15] Pr atoms in SrTiO$_3$ can be in two oxidation states (3+ and 4+). The subsequent synchrotron radiation x-ray diffraction study of a $(Sr_{1-x}Pr_x)TiO_3$ sample with higher Pr concentration ($x = 0.15$) revealed a tetragonal lattice distortion, which was attributed to the appearance of the $P4mm$ phase.[16]

X-ray and neutron powder diffraction studies of the samples with $x \geq 0.09$ by another experimental group[17,18] revealed superstructure peaks in the diffraction patterns, and the structure of the samples was determined to be $I4/mcm$. It was concluded that doping SrTiO$_3$ with Pr increases the temperature of the phase transition to the $I4/mcm$ phase, and at $x = 0.05$ it is close to 300 K.[17] Raman studies of these samples[17,19] revealed weak E_g mode, which originates from the T_{2u} silent mode of the $Pm3m$ phase and becomes Raman active in the $I4/mcm$ phase. Monotonic change of the frequency of the (formally forbidden in the $Pm3m$ phase) soft TO$_1$ mode in Raman spectra of $(Sr_{0.975}Pr_{0.025})TiO_3$ without any features at the temperature of the dielectric anomaly[19] proves the absence of the displacive ferroelectric phase transition in SrTiO$_3$(Pr). Observation of the dielectric relaxation[19] showed that the system can be regarded as a high-temperature relaxor ferroelectric with the temperature of transition to the relaxor state independent of the structural phase transition temperature.[18]

a)E-mail: irinasluch@nm.ru.

Dielectric studies[20] of $(Sr_{1-x}Pr_x)TiO_3$ samples with $0 \leq x \leq 0.03$ revealed a "colossal" room-temperature dielectric constant of about 3000 at 1 KHz in the sample with $x = 0.01$. The results of this work, however, differed considerably from those of previous studies:[15–19] instead of peaks in the real part of the complex dielectric constant $\varepsilon = \varepsilon' + i\varepsilon''$, a monotonic increase of ε' with noticeable inflections accompanied by the corresponding peaks in ε'' were observed in the 0–500 °C temperature range.

To explain the observed dielectric anomaly, several models have been proposed: (1) displacive ferroelectric phase transition in the bulk;[15] (2) appearance of polar nanoregions around various defects such as $Pr^{3+}/Pr^{4+}–V_{Sr}$ complexes, off-center Pr_{Sr} ions, and Ti^{4+} ions displaced as a result of the $Sr \rightarrow Pr$ substitution;[19] (3) capacitive effect arising from the semiconducting nature of grains and insulating grain boundaries in ceramic samples.[20]

In this paper, the crystal structure of Pr-doped $SrTiO_3$, the structural position and the oxidation state of Pr ions, and the mechanisms responsible for maintaining charge neutrality upon heterovalent substitution are studied using x-ray diffraction, extended x-ray absorption fine structure (EXAFS), and x-ray absorption near-edge structure (XANES) techniques. A model of the defect structure which explains main properties of these samples is proposed, and possible interpretations of the dielectric anomaly are critically analyzed.

II. EXPERIMENTAL

Samples with a nominal composition of $(Sr_{1-x}Pr_x)TiO_3$ ($x = 0.05, 0.15,$ and 0.3) and $Sr(Ti_{1-x}Pr_x)O_3$ ($x = 0.05$) were prepared by the solid-state reaction method from $SrCO_3$, Pr_6O_{11}, and nanocrystalline TiO_2 which was synthesized by hydrolysis of tetrapropylorthotitanate and dried at 500 °C. Starting materials were weighed in necessary proportions, mixed, ground under acetone, and calcined in air at 1100 °C for 8 h. The calcined powders were ground once more and annealed again at 1100–1600 °C. The annealing times were 8 h for 1100 °C, 4 h for 1300 and 1400 °C, 2 h for 1600 °C. The temperature of 1100 °C was found insufficient to enter the praseodymium into reaction; solid solutions were formed starting from 1300 °C.

EXAFS and XANES spectra were obtained at KMC-2 station of the BESSY synchrotron radiation source at the Pr L_{II}-edge (6440 eV) and the Ti K-edge (4966 eV) at 300 K. Spectra were collected in fluorescence mode using an energy-dispersive Röntec X-flash detector with 10 mm^2 active area. The choice of the Pr L_{II}-edge instead of the more common L_{III}-edge was motivated by the following. The energies of the Pr $L_{\alpha1}$ fluorescence line (exited at the L_{III}-edge) and of the Ti K_β fluorescence line are very close. This strongly complicates the measurements. Selecting of the Pr L_{II}-edge results in excitation of the $L_{\beta1}$ fluorescence line, whose energy differs by 560 eV from the energy of the Ti K_β fluorescence line. This is sufficient to separate the signals from Pr and Ti atoms. The spectra at the Pr L_{II}-edge were recorded in a limited energy range (6400–6840 eV) because of the proximity of the Pr L_I-edge. EXAFS spectra were processed in two ways. First, they were analyzed in our

traditional way[21] using FEFF6 software[22] for calculating the scattering amplitudes and phases. Second, the data were pre-processed using ATHENA software and were fitted using ARTEMIS software[23] to the theoretical curves computed for a given structural model; in this approach, the scattering amplitudes and phases were also calculated using FEFF6. The results obtained by both methods agreed well.

III. RESULTS

X-ray diffraction studies showed that $Sr(Ti_{0.95}Pr_{0.05})O_3$ samples annealed at 1300–1600 °C were not single-phase; additional peaks of the $Sr_3Ti_2O_7$ Ruddlesden-Popper phase and Pr_6O_{11} were observed in their diffraction patterns. $(Sr_{1-x}Pr_x)TiO_3$ samples with $x = 0.05$–0.15 were single-phase, whereas the sample with $x = 0.3$ contained a small amount of $PrO_{2-\delta}$ and $SrPr_4Ti_5O_{17}$ second phases.

Along with peaks characteristic of the cubic perovskite structure, additional superstructure reflections, whose intensity increased with increasing Pr concentration, were observed in the diffraction patterns of $(Sr_{1-x}Pr_x)TiO_3$ samples with $x = 0.15$–0.3. These peaks are denoted by arrows in Fig. 1 and can be indexed on the cubic lattice as (3/2, 1/2, 1/2), (3/2, 1/2, 3/2), and (5/2, 1/2, 1/2) reflections. Following Glazer,[24] the appearance of these superstructure reflections indicates the rotation of the oxygen octahedra around the c axis according to the $a^0a^0c^-$ tilt system, which results in a lowering of symmetry from cubic $Pm3m$ to tetragonal $I4/mcm$ and in a doubling of the unit cell. Since the structural phase transition to the same phase occurs in undoped $SrTiO_3$ at 105 K, one can conclude that doping $SrTiO_3$ with Pr results in the increase of the phase transition temperature, and this temperature exceeds 300 K in samples with $x \geq 0.15$. This conclusion agrees with that drawn from the neutron diffraction study,[18] but it can be noted that in this work a full set of superstructure reflections was observed in x-ray diffraction.

The lattice parameters of $(Sr_{1-x}Pr_x)TiO_3$ samples annealed at 1400 °C were $a = 3.897$ Å for $x = 0.05$, 3.898 Å for $x = 0.15$, and 3.894 Å for $x = 0.3$.[25] It is seen that the lattice parameter decreases slowly with increasing
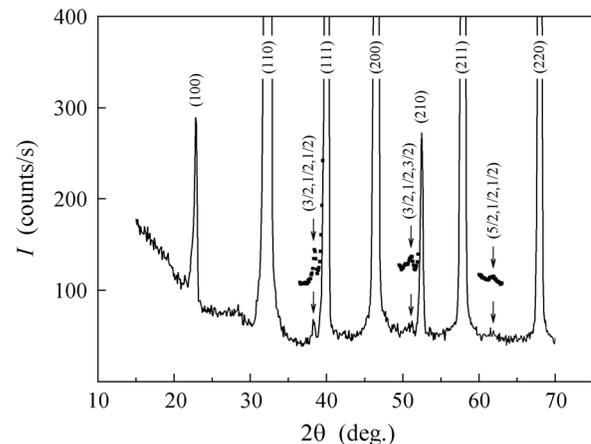

FIG. 1. X-ray diffraction pattern of $(Sr_{0.85}Pr_{0.15})TiO_3$ sample annealed at 1400 °C. Fragments of the diffraction pattern recorded with the integration time of 300 s are shifted along the vertical axis and shown by squares. Calculated positions of the superstructure peaks are denoted by arrows.
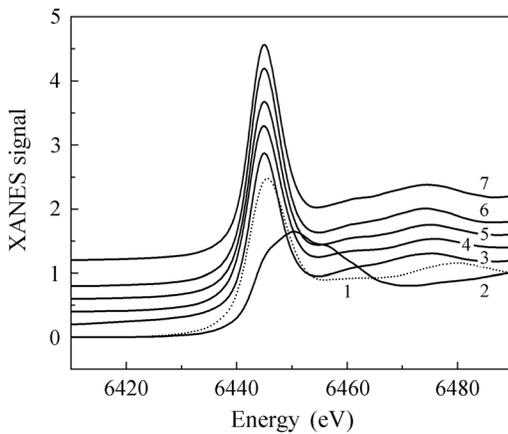
FIG. 2. XANES spectra of $SrTiO_3$(Pr) samples and reference compounds of tri- and tetra-valent praseodymium recorded at the Pr L_{II}-edge at 300 K. 1—$Pr_2Ti_2O_7$, 2—$BaPrO_3$, 3, 6, 7—$(Sr_{0.95}Pr_{0.05})TiO_3$ samples annealed at 1600, 1400, and 1300 °C, respectively, 4—$(Sr_{0.7}Pr_{0.3})TiO_3$ sample annealed at 1400 °C, 5—$(Sr_{0.85}Pr_{0.15})TiO_3$ sample annealed at 1400 °C.

Pr concentration. According to Refs. 15, 17, and 18, the lattice parameter of $(Sr_{1-x}Pr_x)TiO_3$ is nearly independent of x.

To determine the oxidation state of Pr ions in our samples, their XANES spectra were compared with those of the reference compounds. The spectra for five $(Sr_{1-x}Pr_x)TiO_3$ samples and Pr^{3+} and Pr^{4+} reference compounds ($Pr_2Ti_2O_7$ and $BaPrO_3$, respectively) are shown in Fig. 2. Comparison of these spectra shows that the oxidation state of the Pr ion in our samples is predominantly 3+ and does not depend on the Pr concentration and the preparation conditions. This differs from the behavior of the Mn impurity in $SrTiO_3$, whose oxidation state and structural position strongly depended on the preparation conditions.[26,27]

To determine the structural position of the Pr impurity, EXAFS spectra were analyzed. Typical Fourier-filtered EXAFS spectrum as a function of the photoelectron wave vector k for the $(Sr_{0.85}Pr_{0.15})TiO_3$ sample and its best theoretical fit are shown in Fig. 3. The best agreement between the experimental and calculated data was obtained for a model in which the Pr atoms substitute for the Sr atoms. Interatomic
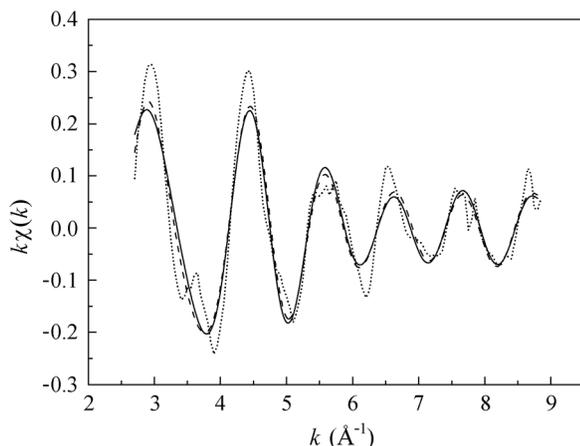
distances and Debye-Waller factors for three nearest shells are given in Table I. Comparison of the obtained interatomic distances with those calculated for an ideal perovskite structure with the lattice parameter taken from x-ray measurements shows that a strong relaxation around the impurity atom occurs only in the first shell (the average relaxation is $\Delta R \approx -0.136$ Å). In contrast, a slight increase in the average interatomic distance ($\Delta R \approx +0.02$ Å) is found in the second shell. In the third shell, the accuracy of determination of the structural parameters is not sufficient to draw any conclusions; however, the interatomic distance for this shell is consistent with x-ray data (Table I).

Small values of the Debye-Waller factors for the second shell (Table I), which are typical for thermal vibrations in perovskites at 300 K, enable to completely exclude the off-centering of the Pr atoms. Unexpectedly large Debye-Waller factor for the first shell in the sample with $x = 0.15$ can be explained by static distortions of the Pr–O bond lengths resulting from the rotation of the oxygen octahedra in the $I4/mcm$ phase. In the sample with $x = 0.05$, high Debye-Waller factor may indicate large thermal fluctuations of the rotation angle because at this Pr concentration, the temperature of the structural phase transition is close to 300 K.[17]

To check for the possibility of the Pr incorporation into the B sites of the perovskite structure, experimental EXAFS spectra were compared with the spectra calculated in the model in which the impurity enters both the A and B sites simultaneously. It turned out that with increasing concentration of Pr at the B sites, the agreement of the curves becomes worse. This means that the incorporation of Pr into the B sites is very unlikely, apparently because of the strong difference in ionic radii of Ti^{4+} (0.605 Å) and Pr^{3+} (0.99 Å) in octahedral coordination.[28]

IV. DISCUSSION

X-ray studies performed in this work confirmed previous results[17,18] that doping $SrTiO_3$ with Pr increases the temperature of the structural phase transition from the cubic $Pm3m$ to the tetragonal $I4/mcm$ phase.

The weak effect of Pr doping on the lattice parameter of $(Sr_{1-x}Pr_x)TiO_3$ is an unusual feature of these samples.[15,17,18] In our x-ray measurements, the decrease of the lattice parameter was less than 0.008 Å in the whole solubility range ($a = 3.905$ Å in bulk $SrTiO_3$).

We compare the interatomic distances obtained from x-ray and EXAFS measurements. The average difference between the x-ray and EXAFS Pr–O distances in the first shell (-0.136 Å) is very close to the difference between ionic radii of Pr^{3+} and Sr^{2+}. Because of the lack of data on the ionic radius of the Pr^{3+} ion in 12-fold coordination, we used the data for 8-fold coordination for both ions, $R_{Sr^{2+}} = 1.26$ Å and $R_{Pr^{3+}} = 1.126$ Å.[28] The difference of these ionic radii, 0.134 Å, coincides with the relaxation in the first shell obtained from our EXAFS measurements.

At the same time, the EXAFS interatomic distances in the second shell turned out a little bit larger than the mean interatomic distances in the perovskite structure. This can be explained as follows. According to the second Pauling's

FIG. 3. EXAFS spectra obtained at the Pr L_{II}-edge at 300 K for $(Sr_{0.85}Pr_{0.15})TiO_3$ sample annealed at 1400 °C. The dashed line shows the Fourier-filtered spectrum ($R = 1.3$–4.0 Å, three nearest shells) and the solid line is its best theoretical fit. The raw data are shown by the dotted line.

TABLE I. Structural parameters obtained from the EXAFS data analysis (R_i is the distance to the i-th shell, σ_i^2 is the Debye-Waller factor for this shell) and mean interatomic distances in the perovskite structure with the lattice parameters taken from x-ray measurements. The R-factor indicates the goodness of fit of the theoretical curves to the Fourier-filtered spectra.

Shell	$(Sr_{0.95}Pr_{0.05})\,TiO_3$ annealed at 1300 °C		$(Sr_{0.95}Pr_{0.05})\,TiO_3$ annealed at 1600 °C		$(Sr_{0.85}Pr_{0.15})\,TiO_3$ annealed at 1400 °C		$(Sr_{0.95}Pr_{0.05})\,TiO_3$, x-ray data
	R_i (Å)	σ_i^2 (Å^2)	R_i (Å)	σ_i^2 (Å^2)	R_i (Å)	σ_i^2 (Å^2)	R_i (Å)
Pr–O	2.629(9)	0.017(1)	2.623(7)	0.014(1)	2.608(15)	0.020(2)	2.756
Pr–Ti	3.394(5)	0.003(1)	3.388(4)	0.003(1)	3.404(8)	0.004(1)	3.375
Pr–Sr	3.887(34)	0.022(5)	3.926(13)	0.012(2)	3.930(38)	0.018(5)	3.897
R-factor	0.0041		0.0037		0.0112		…

rule,[29] the perovskite structure is electrostatically compensated, which means that the sum of the strengths of the electrostatic valence bonds of Sr^{2+} and Ti^{4+} cations which reach the O^{2-} anion is equal to the ionic charge of the anion. Substitution of Sr^{2+} by Pr^{3+} disturbs the local charge compensation and results in the repulsion of positively charged Pr^{3+} and Ti^{4+} ions. So, the Pr–Ti interatomic distance increases. The fact that we did not reveal the incorporation of Pr atoms into the B sites of the perovskite structure excludes the explanation[17] that the weak dependence of the lattice parameter in $(Sr_{1-x}Pr_x)TiO_3$ on x is caused by the partial substitution of Ti^{4+} ions by larger Pr^{3+} ions. In our opinion, this weak dependence is a consequence of two competing effects, the relaxation in the first shell resulting form the difference in ionic radii, and the repulsion of positively charged Pr^{3+} and Ti^{4+} ions.

As the main oxidation state of the Pr ions in our samples is 3+, this implies the existence of some charged defects to maintain charge neutrality of the sample. The vacancies V_{Sr}, V_{Ti}, and V_O can act as such defects, as well as Ti atoms in the 3+ oxidation state.

The possibility of reduction of the Ti ion to Ti^{3+} state can be excluded because otherwise the samples would darken (our samples are light yellow). To clarify the role of the oxygen vacancies, the pre-edge structure at the Ti K-edge in the $(Sr_{0.95}Pr_{0.05})TiO_3$ sample was studied. The experiment did not reveal any increase in the intensity of the $1s \rightarrow 3d$ (e_g) dipole-forbidden transition at 4969 eV (Ref. 30) (Fig. 4), thus indicating that the symmetry of the oxygen octahedra was preserved (the symmetry would be broken by the presence of V_O vacancies). An increase in the intensity of two unresolved peaks at 4972–4975 eV, which are attributed to the dipole-forbidden transitions of the Ti $1s$ electron into the t_{2g} and e_g orbitals of neighboring TiO_6 octahedra,[31] is probably a consequence of the Pr-induced disorder in our samples. The formation of Ti vacancies in our samples is improbable because otherwise the excess of Ti would precipitate as the TiO_2 phase; the peaks of this phase were absent in our x-ray diffraction patterns. Therefore, the most important charged defects that maintain charge neutrality in Pr-doped $SrTiO_3$ are Sr vacancies.

The existence of Sr vacancies in $(Sr_{1-x}Pr_x)TiO_3$ samples with high x implies the precipitation of excess Sr. For example, in the sample with $x = 0.15$, the concentration of V_{Sr} should be equal to 7.5%, so that this amount of excess strontium should be precipitated as an oxide phase which can be

easily detected in x-ray experiments. However, no additional peaks were observed in x-ray diffraction patterns of the $(Sr_{0.85}Pr_{0.15})TiO_3$ sample. At the same time, it is well known that in the $SrTiO_3$–SrO system the excess Sr can form so-called planar faults, which are stacking faults consisting of one extra SrO layer inserted between SrO and TiO_2 layers in the $SrTiO_3$ structure and intergrown coherently with the adjacent layers.[32,33] In the case of a regular arrangement of these extra layers, the structures called the Ruddlesden-Popper phases with a general formula $Sr_{n+1}Ti_nO_{3n+1}$ are formed.[34] The planar faults were observed using electron microscopy even in stoichiometric $SrTiO_3$.[35] In this work, the Ruddlesden-Popper phases were observed in x-ray diffraction only in $Sr(Ti_{1-x}Pr_x)O_3$ samples annealed at temperatures insufficient for dissolving praseodymium. In single-phase $(Sr_{1-x}Pr_x)TiO_3$ samples, we believe that excess Sr forms planar faults as well. But in this case, the absence of the diffraction peaks of the Ruddlesden-Popper phase simply indicates the absence of the long-range order in the arrangement of SrO planar faults. We think that randomly distributed Pr^{3+}–V_{Sr} complexes act as pinning centers for the motion of SrO planar faults, and so their regular arrangement cannot be achieved.

From the previous discussion, it follows that there are two possible positions of Sr atoms in our samples: the Sr sites in the $SrTiO_3$ perovskite layers and the Sr sites in the SrO planar faults. In the Ruddlesden-Popper phases, different impurity atoms substitute for different Sr sites: for
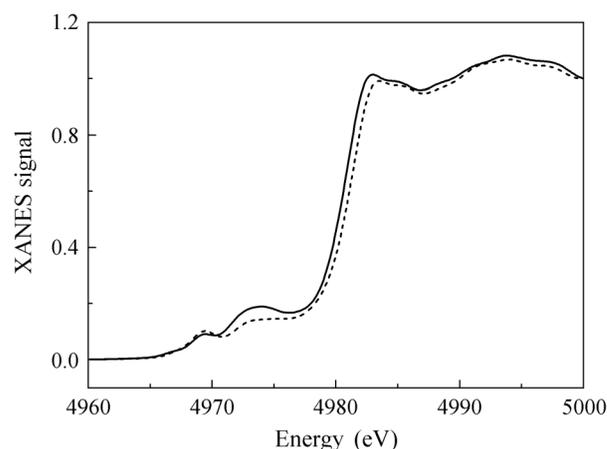

FIG. 4. XANES spectra recorded at the Ti K-edge at 300 K for $(Sr_{0.85}Pr_{0.15})TiO_3$ sample annealed at 1400 °C (full line) and undoped $SrTiO_3$ sample (dashed line).

example, Ba atoms predominantly enter the $SrTiO_3$ layers, thus forming a solid solution,[36] whereas Ca atoms predominantly enter the SrO planar faults.[36,37] To refine the position of the Pr atoms in our heavily doped samples, we additionally analyzed our EXAFS spectra in the model in which Pr atoms substitute for Sr atoms in the SrO planar faults. Initial structural positions of atoms were taken from the crystal structure of the $Sr_3Ti_2O_7$ Ruddlesden-Popper phase. Because of the similarity between the crystal structures of $SrTiO_3$ and the Ruddlesden-Popper phase (a half of the Ruddlesden-Popper-phase structure nearly coincides with the perovskite structure), the calculated EXAFS spectra for these structures were similar. Nevertheless, a better agreement with the experimental EXAFS spectra was obtained for the model in which the Pr atoms substitute for the Sr atoms in the $SrTiO_3$ layers. This is not surprising because to incorporate the Pr atoms into the Sr sites in the SrO planar faults, these planar faults should be first created by the $Sr \to Pr$ substitution in bulk $SrTiO_3$.

The defect model proposed in this work explains the influence of addition of Al and other trivalent impurities (Ga, In, B) on the intensity of the red luminescence in Pr-doped $SrTiO_3$. As was mentioned in Sec. I, co-doping $SrTiO_3$(Pr) with the trivalent impurities can enhance the luminescence efficiency up to 200 times. We think that both Sr vacancies and SrO planar faults act as non-radiative centers in $SrTiO_3$(Pr). The addition of trivalent impurities results in two effects: (1) partial substitution of titanium by trivalent impurity maintains charge neutrality of the samples and excludes the creation of Sr vacancies, and (2) x-ray amorphous phase based on the oxide of trivalent impurity "absorbs" the planar faults. As a result, the addition of trivalent impurity "purifies" the grains of $SrTiO_3$ from point and planar defects, thus creating optimal conditions for radiative recombination.

An increase of the structural phase transition temperature T_s when doping $SrTiO_3$ with Pr is not surprising because the ionic radius of Pr^{3+} is less than that of Sr^{2+}: the decrease of the A atom size in the perovskite structure decreases the tolerance factor, and the instability of the structure against octahedra rotations increases. More surprising is the fact that the dT_s/dx rate for Pr doping is higher than that for Ca doping (the impurities have the same ionic radius). For Pr doping, the temperature T_s reaches 300 K at $x = 0.05$,[17] whereas for Ca doping T_s reaches 300 K only at $x = 0.1$.[6] We believe that such a strong effect of Pr doping on T_s is due to the presence of Sr vacancies which influence the octahedra rotation in a manner similar to the influence of small A cations.

In this work, we considered exclusively the structural properties of Pr-doped $SrTiO_3$ and established that Pr is not an off-center ion and doping with Pr is not accompanied by creation of the oxygen vacancies in TiO_6 octahedra. The weak effect of the Pr concentration on the temperature of the dielectric anomaly[15] and a gradual change of the soft mode frequency at the temperature of this anomaly[19] indicate that this anomaly is not associated with the bulk of the crystal. We think that the model of ferroelectricity in a system of frozen Pr^{3+}–V_{Sr} electric dipoles[19] is also unreasonable because it cannot explain the switching of polarization, and the local

electric fields around defects reduce the lattice susceptibility and therefore can only decrease the Curie temperature.[38] So, none of the models mentioned in Sec. I can explain the appearance of ferroelectricity.

In our opinion, a possible cause of the dielectric anomaly may be the appearance of the conductivity associated either with the ionization of the Pr donor levels ($Pr^{3+} \to Pr^{4+} + e^-$) or with a thermally-assisted hopping of electrons between Pr atoms which can exist in two different oxidation states (Pr^{3+} and Pr^{4+}). Indeed, the results of the recent studies of Pr-doped $SrTiO_3$ using impedance spectroscopy[20] were interpreted using an equivalent circuit consisting of semiconducting grains and insulating grain boundaries. In this case, the dispersion of the dielectric properties is a result of the Arrhenius equation for conductivity of grains.

V. CONCLUSIONS

X-ray diffraction studies confirmed that the structure of $(Sr_{1-x}Pr_x)TiO_3$ solid solutions at 300 K changes from the cubic $Pm3m$ to the tetragonal $I4/mcm$ with increasing x. The analysis of the XANES spectra revealed that the Pr ions are predominantly in the 3+ oxidation state. The analysis of the EXAFS data showed that the Pr atoms substitute for the Sr atoms in $SrTiO_3$ and are on-center regardless of the preparation conditions. The local environment of the Pr impurity (the Pr–O distance) is characterized by a strong relaxation ($\Delta R \approx -0.136$ Å) which is close to the difference of ionic radii of Sr^{2+} and Pr^{3+}. In contrast, in the second shell, a slight increase in the interatomic distance ($\Delta R \approx +0.02$ Å) was revealed and explained by the repulsion of positively charged Pr^{3+} and Ti^{4+} ions. The weak dependence of the lattice parameter in $(Sr_{1-x}Pr_x)TiO_3$ on x is therefore a result of the competition between the relaxation of the first shell and the repulsion in the second shell. Various possible defects providing electrical neutrality of the samples were analyzed and it was shown that the most important defects in Pr-doped $SrTiO_3$ are charged Sr vacancies and SrO planar faults. It was shown that among two possible Sr positions in this defect model (Sr in the $SrTiO_3$ lamella-type layers and Sr in the SrO planar faults), the Pr atoms predominantly incorporate into the $SrTiO_3$ layers.

ACKNOWLEDGMENTS

[1]S. Okamoto, H. Kobayashi, and H. Yamamoto, J. Appl. Phys. **86**, 5594 (1999).
[2]S. Okamoto and H. Yamamoto, Appl. Phys. Lett. **78**, 655 (2001).
[3]H. Landolt and R. Börnstein, *Landolt-Börnstein. Numerical Data and Functional Relationships in Science and Technology. New Series. Group III* (Springer-Verlag, 2001), Vol. 36A1.
[4]J. Hemberger, M. Nicklas, R. Viana, P. Lunkenheimer, A. Loidl, and R. Böhmer, J. Phys.: Condens. Matter **8**, 4673 (1996).
[5]H. Uwe and T. Sakudo, Phys. Rev. B **13**, 271 (1976).
[6]T. Mitsui and W. B. Westphal, Phys. Rev. **124**, 1354 (1961).
[7]J. G. Bednorz and K. A. Müller, Phys. Rev. Lett. **52**, 2289 (1984).

[8]V. V. Lemanov, E. P. Smirnova, P. P. Syrnikov, and E. A. Tarakanov, Phys. Rev. B **54**, 3151 (1996).

[9]M. Itoh, R. Wang, Y. Inaguma, T. Yamaguchi, Y.-J. Shan, and T. Nakamura, Phys. Rev. Lett. **82**, 3540 (1999).

[10]V. V. Lemanov, in *Defects and Surface-induced Effects in Advanced Perovskites*, edited by G. Borstel, A. Krumins, and D. Millers (Kluwer Academic Publishers, 2000), pp. 329–340.

[11]M. E. Guzhva, V. V. Lemanov, and P. A. Markovin, Phys. Solid State **43**, 2146 (2001).

[12]V. V. Lemanov, E. P. Smirnova, A. V. Sotnikov, and M. Weihnacht, Phys. Solid State **46**, 1442 (2004).

[13]V. V. Lemanov, A. V. Sotnikov, E. P. Smirnova, and M. Weihnacht, J. Appl. Phys. **98**, 056102 (2005).

[14]C. Ang, Z. Yu, P. Lunkenheimer, J. Hemberger, and A. Loidl, Phys. Rev. B **59**, 6670 (1999).

[15]A. Duran, E. Martinez, J. A. Diaz, and J. M. Siqueiros, J. Appl. Phys. **97**, 104109 (2005).

[16]A. Duran, F. Morales, L. Fuentes, and J. M. Siqueiros, J. Phys.: Condens. Matter **20**, 085219 (2008).

[17]R. Ranjan, R. Garg, R. Hackl, A. Senyshyn, E. Schmidbauer, D. Trots, and H. Boysen, Phys. Rev. B **78**, 092102 (2008).

[18]R. Garg, A. Senyshyn, H. Boysen, and R. Ranjan, Phys. Rev. B **79**, 144122 (2009).

[19]R. Ranjan, R. Hackl, A. Chandra, E. Schmidbauer, D. Trots, and H. Boysen, Phys. Rev. B **76**, 224109 (2007).

[20]C. Liu, P. Liu, J.-P. Zhou, Y. He, L.-N. Su, L. Cao, and H.-W. Zhang, J. Appl. Phys. **107**, 094108 (2010).

[21]A. I. Lebedev, I. A. Sluchinskaya, V. N. Demin, and I. H. Munro, Phys. Rev. B **55**, 14770 (1997).

[22]See http://leonardo.phys.washington.edu/feff/ for Feff project home page.

[23]See http://cars9.uchicago.edu/ifeffit/ for Ifeffit project home page.

[24]A. M. Glazer, Acta Crystallogr. A **31**, 756 (1975).

[25]The a and c parameters of the tetragonal phase were so close that they could not be determined independently. Therefore, we considered the unit cell as a pseudocubic one.

[26]A. I. Lebedev, I. A. Sluchinskaya, A. Erko, and V. F. Kozlovskii, JETP Lett. **89**, 457 (2009).

[27]I. A. Sluchinskaya, A. I. Lebedev, and A. Erko, Bull. Russ. Acad. Sci.: Phys. **74**, 1235 (2010).

[28]R. D. Shannon, Acta Crystallogr. A **32**, 751 (1976).

[29]L. Pauling, J. Am. Chem. Soc. **51**, 1010 (1929).

[30]A. I. Lebedev, I. A. Sluchinskaya, A. Erko, A. A. Veligzhanin, and A. A. Chernyshov, Phys. Solid State **51**, 991 (2009).

[31]R. V. Vedrinskii, V. L. Kraizman, A. A. Novakovich, P. V. Demekhin, and S. V. Urazhdin, J. Phys.: Condens. Matter **10**, 9561 (1998).

[32]M. A. McCoy, R. W. Grimes, and W. E. Lee, Philos. Mag. A **75**, 833 (1997).

[33]S. Šturm, A. Rečnik, C. Scheu, and M. Čeh, J. Mater. Res. **15**, 2131 (2000).

[34]S. N. Ruddlesden and P. Popper, Acta Crystallogr. **11**, 54 (1958).

[35]R. J. D. Tilley, J. Solid State Chem. **21**, 293 (1977).

[36]S. Šturm, M. Shiojiri, and M. Čeh, J. Mater. Res. **24**, 2596 (2009).

[37]M. Fujimoto, T. Suzuki, Y. Nishi, K. Arai, and J. Tanaka, J. Am. Ceram. Soc. **81**, 33 (1998).

[38]A. I. Lebedev and I. A. Sluchinskaya, Fiz. Tverd. Tela **35**, 629 (1993).